

Particle-tracking simulation for the drift/diffusion of spilled oils in the Sea of Okhotsk with a three-dimensional, high-resolution model

Jun Ono · Kay I. Ohshima · Keisuke Uchimoto ·
Naoto Ebuchi · Humio Mitsudera · Hajime Yamaguchi

Received: 18 July 2012/Revised: 11 May 2013/Accepted: 16 May 2013/Published online: 19 June 2013
© The Oceanographic Society of Japan and Springer Japan 2013

Abstract To conduct the simulation of oil spills in the Sea of Okhotsk, we developed a three-dimensional, high-resolution ocean circulation model. The model particularly improved the reproducibility of velocity field during the strong stratification period. Particle-tracking experiments with the effects of evaporation and biodegradation were performed using the combined data of daily ocean currents from the present model and the hourly diurnal tidal currents from the tidal model. The results are shown by the relative concentration of the particles averaged over the 8 years of 1998–2005 based on the ensemble forecast idea. For the case of particles released from the Sakhalin II oil field, the particles deployed in September–January are carried southward by the East Sakhalin Current, finally arriving at the Hokkaido coast, after 60–90 days. The particles deployed in March–August are diffused offshore by the synoptic wind drift, and hardly transported to regions south of Sakhalin. For the case of particles released from the region off Prigorodnoye, the oil export terminal, after the diffusion by the synoptic wind drift, a part of them are carried offshore of Hokkaido by the Soya Warm Current.

The particles released in November–April flow out to the Japan Sea through the Soya Strait, mainly by the synoptic wind drift and secondly by the diffusion due to strong tidal currents around the Soya Strait. By considering the effects of evaporation and biodegradation, the relative concentration of the particles is considerably decreased before arriving at the Hokkaido coast, particularly in the case of drift from the Sakhalin II oil field.

Keywords Sea of Okhotsk · East Sakhalin Current · Soya Warm Current · Spilled oil · Particle-tracking experiment

1 Introduction

Oil spill accidents from tankers and offshore platforms are one of the serious problems that affect the marine environment and ecosystem. A serious oil spill incident occurred in the Japan Sea from the Russian tanker *Nakhodka* in January 1997. This incident has promoted the development of an oil spill simulation system for the Japan Sea (Varlamov et al. 1999). Furthermore, an operational simulation model has also been developed by Varlamov and Yoon (2003). These studies showed that ocean currents at depths of 0–15 m play the most important role in the drift/diffusion of spilled oil and that the reproduction of the current field including synoptic variability is the most important for oil spill simulation. As for the numerical simulation of spilled oil, Kakinuma and Yanagi (1976) and Yanagi and Okamoto (1984), who conducted the simulation for the Seto Inland Sea, were the early studies around Japan. In the Sea of Okhotsk, where the Sakhalin oil field exists, an oil spill simulation model was developed by the Petroleum Association of Japan (2005) in accordance with the demand for an operational prediction model. Although

J. Ono (✉) · H. Yamaguchi
Graduate School of Frontier Sciences, The University of Tokyo,
Kashiwanoha 5-1-5, Kashiwa, Chiba 277-8561, Japan
e-mail: jo@1.k.u-tokyo.ac.jp

J. Ono
National Institute of Polar Research, Tachikawa, Tokyo, Japan

K. I. Ohshima · N. Ebuchi · H. Mitsudera
Institute of Low Temperature Science, Hokkaido University,
Sapporo, Hokkaido, Japan

K. Uchimoto
Research Institute of Innovative Technology for the Earth,
Kizugawa, Kyoto, Japan

the model incorporates the effect of wind drift reasonably, the background ocean current in the model is based on schematics from the old Russian and Japanese literature with no seasonal variation, which is quite different from the reality.

The ocean current field in the Sea of Okhotsk has been revealed by observations from the 1990s, particularly by the intensive current measurements carried out in 1998–2001 under the Joint Japanese–Russian–US Study of the Sea of Okhotsk. Surface drifter observations (Ohshima et al. 2002) quantitatively revealed the existence of a southward current along the eastern coast of Sakhalin, called the East Sakhalin Current (ESC). Ohshima et al. (2002) further showed that the ESC consists of two cores: the nearshore core on the shelf and the offshore core over the shelf slope. From long-term mooring measurements (Mizuta et al. 2003), the total transport of the southward ESC at 53°N was estimated to be 6.7 Sv ($1 \text{ Sv} = 10^6 \text{ m}^3 \text{ s}^{-1}$) as an annual average, corresponding to 20–30 % of the Kuroshio and to about 3 times of the Tsushima Warm Current in the Japan Sea. This is because the flow of the ESC extends from the surface to the bottom. The ESC is characterized by the strong seasonal variation of its volume transport, with a maximum in winter and a minimum in summer.

The Soya Warm Current (SWC) is another major ocean current in the Sea of Okhotsk. The SWC is driven by the sea level difference between the Japan Sea and the Sea of Okhotsk and flows southeastward along the coast of Hokkaido in the Sea of Okhotsk through the Soya Strait (Aota 1975; Ohshima 1994; Ohshima and Wakatsuchi 1990). The SWC carries the Kuroshio water entering the Japan Sea via the Tsushima Warm Current into the Sea of Okhotsk. Ebuchi et al. (2006) showed, from high frequency (HF) ocean radars, that the SWC exhibits clear seasonal variations with a maximum velocity in summer and a minimum velocity in winter. Using a bottom-mounted acoustic Doppler current profiler (ADCP), Fukamachi et al. (2008) revealed that the SWC becomes stronger near the surface in summer to fall and stronger near the bottom in winter to spring. Fukamachi et al. (2008, 2010) further showed that the SWC volume transport is 0.7–1.0 Sv as an annual average on the basis of both the vertical structure observed by the ADCP and the horizontal structure observed by the HF ocean radars.

To simulate the drift/diffusion of spilled oil in the Sea of Okhotsk, a model with a good reproduction of ocean currents is indispensable. The above-mentioned observations can be useful comparison data for developing such a model. Simizu and Ohshima (2006) developed a three-dimensional circulation model in the Sea of Okhotsk and succeeded for the first time in reproducing to some extent the structure and seasonal variation of the ESC. Using their

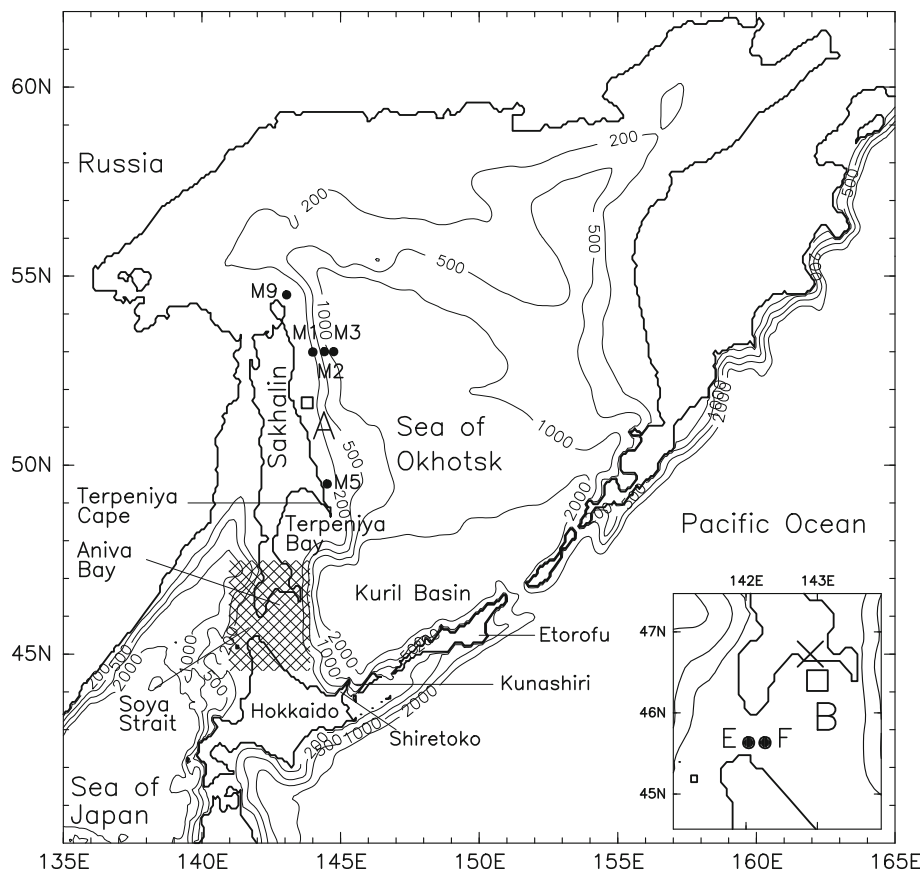
simulated velocity data, Ohshima and Simizu (2008) and Ohshima et al. (2008) conducted a series of particle-tracking experiments, which was the first reliable tracking experiment with good reproduction of the observations. However, their model cannot represent the current structure in the strong stratification period very well, because of the lack of Amur River flux and the coarse resolution of $1/6^\circ$ (about 10–20 km). Moreover, all straits are closed and thus the SWC and water exchange with the Japan Sea and North Pacific were neglected. Uchimoto et al. (2007) developed an Sea of Okhotsk model with finer resolution and water exchange, but used monthly-mean data as the model forcing, which could not represent the synoptic variability, which is important for drift/diffusion of spilled oil. Simizu and Ohshima (2006) and Uchimoto et al. (2007) also did not include the effects of tide and sea ice in their models. Regarding the inclusion of sea ice, Watanabe et al. (2004) developed a coupled ice–ocean model for the Sea of Okhotsk with the resolution being 0.25° in latitude and 0.5° in longitude.

On the basis of the model by Uchimoto et al. (2007), in this study, we develop a three-dimensional, high-resolution ocean circulation model with good reproducibility in the Sea of Okhotsk, by comparison with all the available new and historical data. We also use the tidal current data from a three-dimensional, high-resolution tidal simulation by Ono and Ohshima (2010). Using the combined data of ocean currents and tidal currents, we perform a series of particle-tracking experiments. Specifically, we release particles from the Sakhalin II (rectangular box A in Fig. 1) and the region (rectangular box B in Fig. 1) off Prigorodnoye (cross in Fig. 1), toward a spilled oil prediction in the Sea of Okhotsk. In April 2010, a catastrophic oil spill incident occurred in the Gulf of Mexico (e.g., Kerr et al. 2010). The risk of an oil spill incident also exists in the Sakhalin II, where extensive oil and gas fields have been exploited. In addition, the risk of an oil spill accident due to heavy tanker traffic is relatively high in the region off Prigorodnoye, which is the oil export terminal located at the end of oil and gas pipelines. For these reasons, we select these two areas as the particle-release areas for the particle-tracking experiments in Sect. 4.

2 Model description

The model developed in this study is based on a three-dimensional, high-resolution ocean circulation model by Uchimoto et al. (2007). Their model was constructed from the Japan Coastal Ocean Predictability Experiment (JCOPE; see <http://www.jamstec.go.jp/frgc/jcope/>) (e.g., Miyazawa et al. 2004) which is based on a general coordinate version of the Princeton Ocean Model (Mellor et al. 2002).

Fig. 1 Model geometry. *Solid circles* ($M1$, $M2$, $M3$, $M5$, and $M9$) denote the mooring locations. *Shading* denotes the region of the enlarged map near the Soya Strait. *Solid circles* (E , F) indicate locations used for comparison with the HF ocean radars. A *cross* in the enlarged map indicates Prigorodnoye, which is the oil export terminal. Two *rectangular boxes* A and B show the area in which the particles are released in the particle-tracking experiments in Sect. 4



Zonal and meridional grid spacings are $1/12^\circ \times 1/12^\circ$, corresponding to about 5×10 km on average. The resolution is two times finer than that of the model by Simizu and Ohshima (2006). The vertical grid uses a z - σ coordinate with 45 levels, which takes the σ coordinate below half of the total depth and z coordinate above half at each grid point.

Figure 1 shows the model domain with bottom topography based on the data of GETECH DTM5 and Hydrographic Department of Japan. The model includes the water exchange with the Japan Sea and North Pacific, which is one advantage when compared with the model by Ohshima and Simizu (2008). To reduce the pressure gradient error (Mellor et al. 1994), the bottom topography is smoothed so that the bottom slope between adjacent two grid points, $|H_1 - H_2|/|H_1 + H_2|$ (where H_1 and H_2 are the depths of the adjacent two grid points), is not beyond 0.175. Furthermore, we improved coastal lines and vertical levels near the surface in the model by Uchimoto et al. (2007) as follows: (1) we added the cape located at the tip of the Sakhalin Island around Terpeniya Bay (Fig. 1), and (2) we increased the vertical resolution in the upper layer from (0, 10, 21, and 34 m,...) to (0, 4, 8, 13, 18, and 24 m,...). The level-2.5 turbulence closure scheme (Mellor and Yamada 1982) is used for the vertical eddy viscosity and diffusivity.

The horizontal eddy viscosity and diffusivity are calculated using a formula proportional to the horizontal grid size and velocity gradients (Smagorinsky 1963); the proportionality coefficient is chosen to be 0.2.

After spinup of about 10 years with monthly-mean climatology forcing for wind stress and heat flux, the model is driven by 6-hourly wind stress, 6-hourly heat flux, and monthly-mean fresh water from the Amur River (Ogi et al. 2001). As pointed out by Varlamov et al. (1999) and Ohshima and Simizu (2008), the daily wind forcing including synoptic variability is important for an adequate simulation of drifting materials. Since Uchimoto et al. (2007) used monthly-averaged wind stress, we newly calculated the wind stress using 6-hourly wind data at 10 m above the sea surface from the European Centre for Medium-Range Weather Forecasts Re-Analysis data (ERA-40) with latitude and longitude resolutions of 1.125° from 1998 to August 2002 and the ERA-Interim data with those of 1.5° from September 2002 to July 2006. Following Ohshima et al. (2004) and Simizu and Ohshima (2006), the wind speeds from the ERA-40 and ERA-Interim are corrected by a factor of 1.25 for the whole area. Then, the corrected wind speeds are converted to wind stresses with a formulation by Large and Pond (1981). From 1998 to August 2003, we use heat flux data calculated from NCEP/NCAR reanalysis

dataset combined with the QuikSCAT winds using the bulk formula, while from September 2003, we use the 1-year cycle flux data averaged over 5 years from 1998 to 2002. In addition, salinity at the surface is restored to the monthly mean climatology with a relaxing time constant of 30 days. The climatology of Levitus et al. (1994) used in the model by Uchimoto et al. (2007) did not include high salinity water associated with the sea ice production in the north-west shelf and low salinity water from the Amur River, with the coarse resolution of $1^\circ \times 1^\circ$. Thus, we newly constructed a dataset for monthly-averaged sea surface salinity with a resolution of $1/12^\circ \times 1/12^\circ$, using all the available historical data and newly obtained data by the recent projects and profiling floats (Ohshima et al. 2010). The model is integrated from January 1998 to July 2006. These results will be used as the velocity data for the particle-tracking experiments in Sect. 4. Lateral boundary conditions at the Japan Sea and North Pacific are given by the interpolation from the JCOPE output data with 5-day intervals from January 1998 to 17 September 2003, and from the 1-year cycle JCOPE data averaged over 5 years from 1998 to 2002 thereafter.

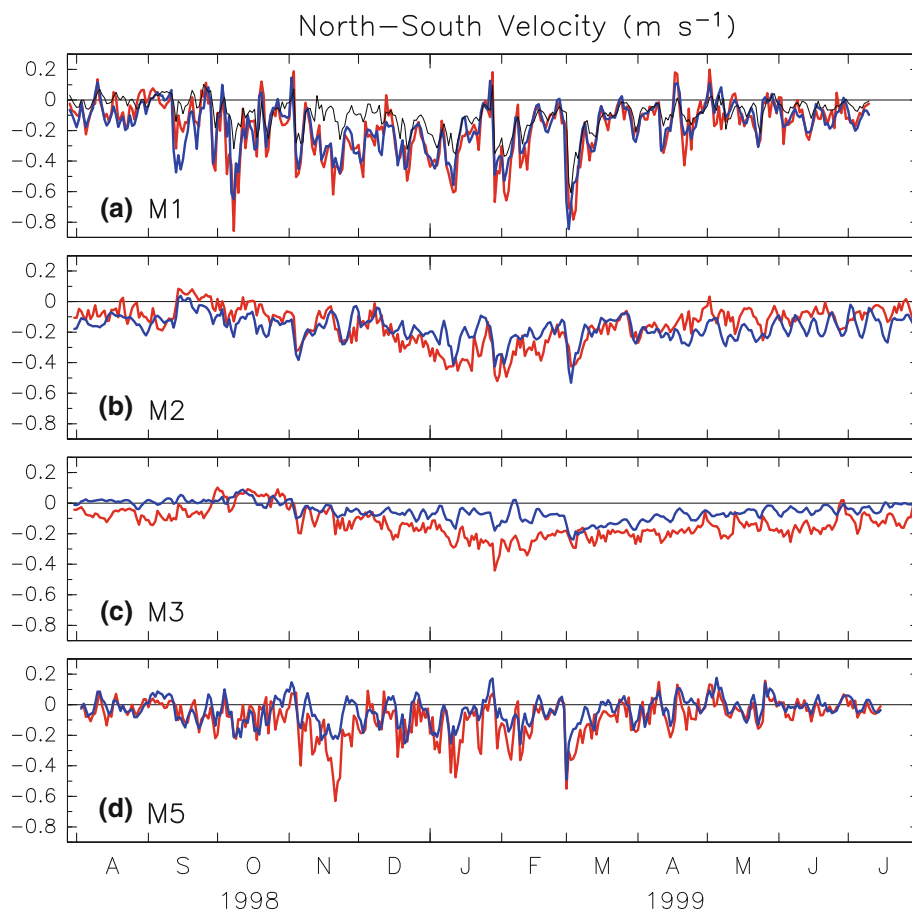
The Sea of Okhotsk is a region of strong diurnal tidal currents and is covered by sea ice in winter. These effects

should be incorporated into the model. In particular, diurnal tidal currents by coastal-trapped waves with amplitudes of $0.2\text{--}0.4\text{ m s}^{-1}$ are dominant over the shelves around the Sakhalin II (Ono et al. 2008). Thus, tidal currents may influence the behavior of drifting materials. In this study, we considered only the diurnal tidal currents (K_1 and O_1), given by harmonic constants calculated from a three-dimensional model by Ono and Ohshima (2010). According to Ohshima and Simizu (2008), the neglect of sea ice in the model is not a significant problem for reproduction of the current over the shelves. Thus, we did not include the dynamics of sea ice in the present model. Actually, the model reproduces the velocity field well in the ice-covered season (January–April), as will be shown in Sect. 3.

3 Model reproducibility

In this section, we examine the reproducibility of the model from comparison with the observations by the ADCPs, current meters, HF ocean radars, and surface drifters. Figure 2 shows the time series of the simulated (blue) and the observed (red) north–south velocities at the mooring sites off the east coast of Sakhalin (see Fig. 1 for

Fig. 2 Time series of north–south velocity at **a** M1 (50 m), **b** M2 (200 m), **c** M3 (100 m), and **d** M5 (50 m), simulated in the model (blue), and measured with bottom-mounted ADCP (at M1 and M5) and current meter (at M2 and M3) (red). For comparison, the model velocity at M1 by Simizu and Ohshima (2006) is superimposed by a thin black line. Daily averaged values are plotted and the northward component is taken as positive (color figure online)



the mooring sites). The model reproduces the observed velocities very well at M1 (Fig. 2a) and M5 (Fig. 2d). From the correlation coefficient, bias, and standard deviation of the daily north–south velocities between the mooring data and model results (Table 1), we find that agreement at M1 is quite good throughout the period. The model even reproduces the variability associated with the synoptic disturbances. As in the model by Ohshima and Simizu (2008), our model shows good agreement in the ice-covered period (January–April), which implies that the inclusion of sea ice in the model is not necessarily important for reproducibility of the current over the shelf. One improved point is the better reproduction of the surface velocity along the east Sakhalin coast during the strong stratification period (May–November). This is because the stratification structure is maintained by giving the Amur River flux and the increase of the vertical resolution. In the previous model (Ohshima and Simizu 2008), that surface velocity is underestimated during that period (thin black line in Fig. 2a). The model also reproduces to some extent the current variability at M2, M3, and M9 (Fig. 2b, c; Table 1). We also compared the model velocities with the surface drifter velocities (Ohshima et al. 2002), as in Ohshima and Simizu (2008). The correlation coefficient between them is significant with a value of 0.60. The simulated southward velocity is smaller by 1.5 cm s^{-1} than the observed one and the standard deviation of the difference between them is 13 cm s^{-1} .

As Simizu and Ohshima (2006) and Ohshima and Simizu (2008) have shown, extremely good reproduction over the shelves (M1 and M5) can be explained by the dynamics of Arrested Topographic Waves (ATWs), that is a coastal current driven by the alongshore wind stress (Csanady 1978). The volume transport by ATWs is the sum of all backward Ekman transport to or from the coast. The southward transport over the shelf shallower than 300 m at

50°N in the model agrees well with that by ATWs (not shown), as in the results of Ohshima and Simizu (2008).

To examine the reproduction of the velocity near the Soya Strait, we compared the surface velocity simulated by our model with that observed by the HF ocean radars (Ebuchi et al. 2006, 2009) near the Soya Strait (see Fig. 1 for the locations). The results of comparison for the east–west component are shown in Fig. 3. Statistical values of the comparisons are listed in Table 1. The model reproduces the variability associated with the synoptic disturbances as well as the seasonal variation. Furthermore, our model reproduces the temporal westward current with the synoptic disturbances in winter (January–February), as observed by the HF ocean radars. Thus, the particle-tracking experiments from coastal regions of Sakhalin and Hokkaido are expected to provide reliable results.

Figure 4 shows the simulated monthly-averaged velocity at the surface, averaged for 8 years. Onset of the intensification of the ESC occurs in October and the southward ESC along the eastern coast of Sakhalin is a dominant feature until March. On the other hand, the southeastward SWC along the coast of Hokkaido is predominant from June to November. Another dominant feature is an anticyclonic circulation in the Kuril Basin. This circulation would exist throughout the year although the northward component on the western side is cancelled by the southward ESC during November–February, when the ESC is strong. Using the combined data of the daily ocean currents from the present model and the hourly tidal currents from the model by Ono and Ohshima (2010), we will conduct the particle-tracking experiments in Sect. 4.

4 Particle-tracking experiments

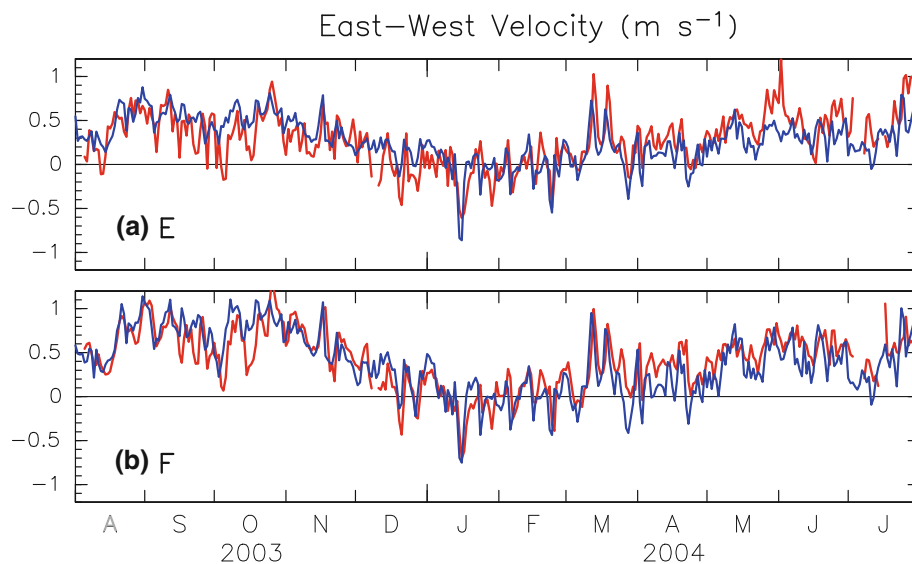
It has been found that the ocean current at the surface is the most important element for the drift/diffusion of spilled oil

Table 1 Comparison of the model velocity with the bottom-mounted ADCP (M1, M5, and M9), current-meter (M2 and M3), and HF ocean radar (E and F) velocity

Site	Depth (m)	Level (m)	Period	Correlation coefficient	Bias (cm s^{-1})	dSTD (cm s^{-1})	Mean (cm s^{-1})	STD (cm s^{-1})
M1	100	50	28 Jul 1998–9 Jul 1999	0.87	0.5	8.7	−17.8	17.6
M2	480	200	30 Jul 1998–1 Jan 2000	0.65	−2.9	9.2	−14.1	12.1
M3	970	100	30 Jul 1998–5 Sep 1999	0.75	8.2	6.6	−13.0	9.0
M5	130	50	2 Aug 1998–14 Jul 1999	0.71	4.6	8.4	−8.5	11.9
M9	90	30	20 Sep 1999–31 Dec 1999	0.72	−6.0	11.6	−19.4	15.2
E	40	0	5 Aug 2003–31 Jul 2004	0.66	−1.0	23.6	28.0	30.1
F	47	0	5 Aug 2003–31 Jul 2004	0.78	−3.3	23.0	41.8	33.2

Correlation, bias, and standard deviation of the difference (*dSTD*) are calculated for the north–south (M1, M2, M3, M5, and M9) and east–west (E and F) components on a daily basis. The mean and standard deviation (*STD*) of the bottom-mounted ADCP, current-meter, and HF ocean radar velocity are also shown in the righthand columns

Fig. 3 Time series of surface velocity at E (a) and F (b) near the Soya Strait (see Fig. 1 for the locations), simulated in the model (blue) and measured with HF ocean radars (red). Daily averaged values of east–west component are plotted with the eastward component being positive (color figure online)



(Varlamov et al. 1999). The spilled oil is not a simple passive tracer. In reality, the movement and behavior of spilled oil are affected by the inherent processes of the spilled oil such as evaporation, dissolution, emulsion, biodegradation, and settling (e.g., Shen and Yapa 1988; Korotenko et al. 2004). However, some of the parameters needed for these processes have not been well understood in the Sea of Okhotsk. According to the document by the Sakhalin Energy Investment Company Ltd. (see http://sakhalinenergy.jp/en/documents/Corporate_OSJ_jap.pdf, in Japanese), the Sakhalin oil has relatively large volatile components. In this case, the oil evaporation proceeds rapidly, causing the increase of oil viscosity. This property and the cold water condition in the Sea of Okhotsk result in the formation of a relatively stable water-in-oil emulsion. Under such conditions, the spilled oil is mainly drifted by the surface ocean currents. Therefore, as a first step, we performed the particle-tracking experiments in which the particles are treated as passive tracers. In addition, we incorporate the effects of evaporation and biodegradation by a simple method as will be described in Sect. 4.1.

4.1 Methods

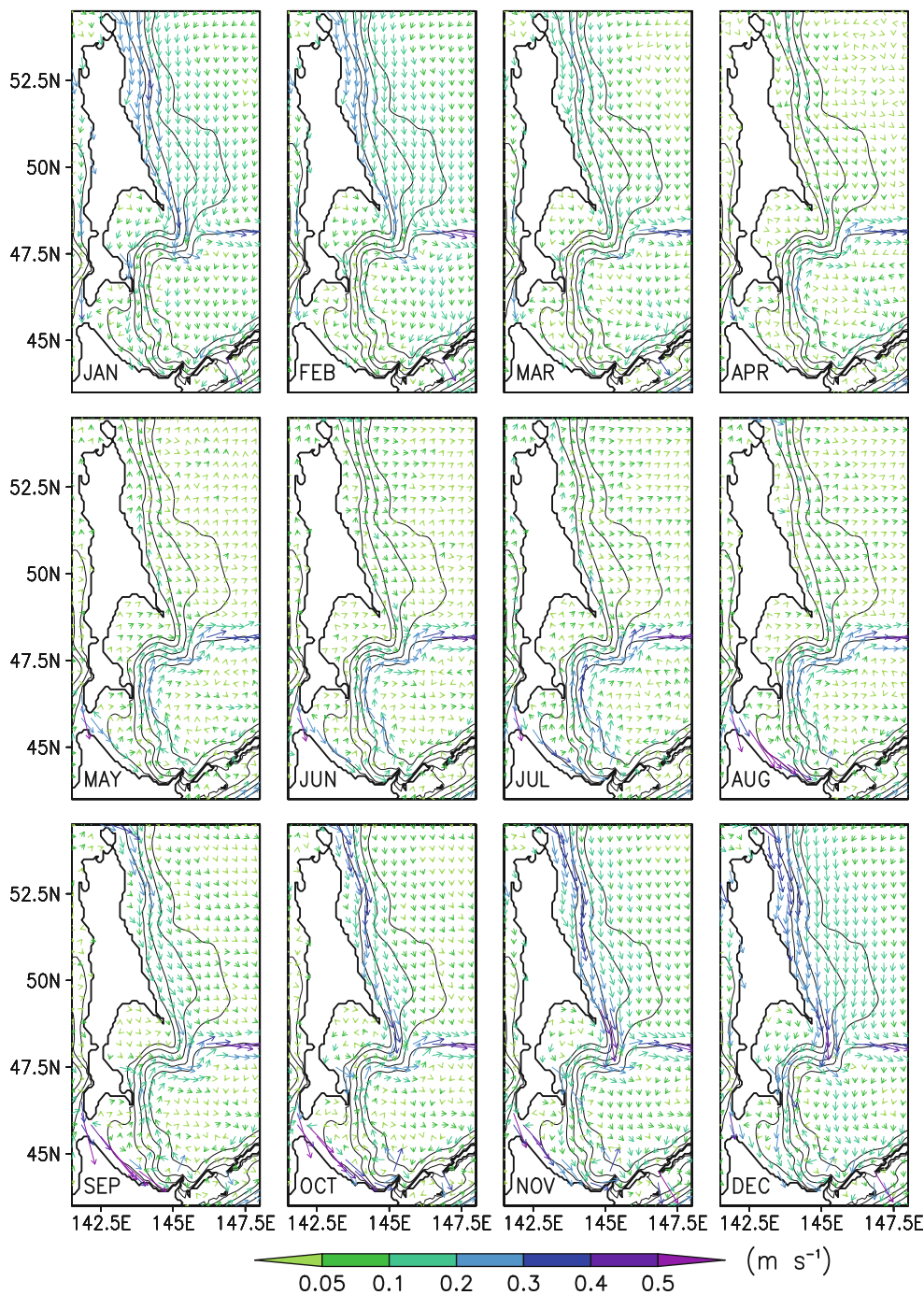
The particle-tracking method is similar to that of Ohshima and Simizu (2008). The new position of a particle at a certain grid cell is calculated hourly by velocity interpolated from velocities at four grid points around the particle. The data used in the particle tracking are daily mean velocity and hourly diurnal tidal currents (K_1 and O_1), from January 1998 to July 2006 at the surface. To check the difference due to the time resolution of the model result, we ran several tests using 2-hourly velocity data from the

model result for calculating the trajectories, and found that the change of time resolution gives no significant change.

We used a random-walk assuming a Markov-chain model to incorporate the smaller spatial and temporal variations than those by wind and tidal currents. In our experiments, we used 1 day as the integral time scale, based on the estimation from the surface drifters (Ohshima et al. 2002). As the horizontal turbulent diffusivity, we used $1.0 \times 10^5 \text{ cm}^2 \text{ s}^{-1}$, which is one-tenth of that used in Ohshima and Simizu (2008), since the tidal effects are explicitly included in our experiments. We also ran several simulations using 10^4 and $10^6 \text{ cm}^2 \text{ s}^{-1}$ as the horizontal turbulent diffusivity, and found that the change of horizontal turbulent diffusivity gives no significant change. It has been reported that more than 90 % of oil stays in the 0–3 m surface layer (Guo and Wang 2009). In the present particle-tracking experiments, we assumed that the spilled oil remains within the surface (first) layer of 0–4 m and that the vertical movement of the particle is neglected.

To investigate the drift/diffusion of spilled oil from the Sakhalin II (rectangular box A in Fig. 1) and the region off Prigorodnoye (rectangular box B in Fig. 1), we conducted particle-tracking experiments with the start at the beginning of each month during 1998–2005. In all experiments, 500 particles, evenly spaced in a rectangular box, A or B, are deployed every day for the initial 30 days and tracked for 150 days. To incorporate the spilled oil evaporation and biodegradation processes that were not included in Ohshima and Simizu (2008), we defined the tracer concentration $C_i(t)$ at time t (in h) for the i -th particle. The initial value of $C_i(0)$ is set unity and $C_i(t)$ is calculated as $C_i(t) = \exp(-\{\lambda_{\text{evp}} + \lambda_{\text{bio}}\}t)$, where the values of λ_{evp}

Fig. 4 Simulated monthly-averaged velocity at the surface, averaged for the 8 years of 1998–2005. Model coastlines and bottom contours of 100, 200, 500, 1,000, and 2,000 m are denoted by *thick* and *thin* lines, respectively



and λ_{bio} are defined by $\ln(2)/\tau_{\text{evp}}$ and $\ln(2)/\tau_{\text{bio}}$ using half-life τ_{evp} and τ_{bio} for evaporation and biodegradation, respectively. In this study, half-life τ_{evp} and τ_{bio} are set to 25 and 250 h, respectively, following Varlamov et al. (1999). The evaporation is assumed to stop after the elapsed time of $3\tau_{\text{evp}}$ (=75 h), considering that the less volatile components remain due to changes in oil properties with time, while the biodegradation is assumed to continue throughout the particle-tracking experiments (Varlamov

et al. 1999). Therefore, the tracer concentration at $t > 3\tau_{\text{evp}}$ is reduced to $C_i(t) = \exp(-3\lambda_{\text{evp}}\tau_{\text{evp}} - \lambda_{\text{bio}}t)$.

The ratio of the sum of the tracer concentration of the particles at a certain grid cell relative to the sum of total initial tracer concentration of released particles is defined as the relative (tracer) concentration of the particles $D(\%)$. Thus, D at a certain grid cell is calculated as $\sum C_i(t)/N \times 100$, where N is the total number (500 for $t = 24$ h, 1,000 for $t = 48$ h, ..., and 15,000 for $t \geq 720$ h) of

released particles, and $\sum C_i(t)$ is the sum of the tracer concentration of the particles found in that grid cell out of N . Since $C_i(0)$ is initially set to unity, the sum of the initial tracer concentration of the total particle released equals N . For example, if the 10th particle and the 50th particle are found in that certain grid cell at time t after the deployment of 500 particles, the relative concentration D is calculated as $(C_{10}(t) + C_{50}(t))/500 \times 100$. Finally, the relative concentration is averaged over 8 years of different velocity fields, based on the ensemble forecast idea.

When spilled oil reaches the coast, it remains at the coast or separates from the coast. This process (hereafter the beaching effect) should be parameterized in the model. In real conditions, however, the beaching effect is thought to depend on the character of the coastal zone and the properties of the spilled oil. In this study, for simplicity, the particles at the coast are treated with the following two extreme ways: (1) when a particle reaches the coast, it is forcibly returned to the position at the previous time step from the coast (hereafter non-beaching case), and (2) once

a particle reaches the coast, it would remain at the coast (hereafter beaching case). The evaporation and biodegradation processes are assumed to stop for the beached particles.

4.2 Particle-tracking simulations off the Sakhalin II

Figure 5a, b shows the simulated relative concentrations at the surface after 30, 60, and 90 days in the case of April deployment, where the total of 15,000 particles were released from the Sakhalin II in April. In the non-beaching case (Fig. 5a), the particles are diffused north–southward and offshoreward by the wind drift due to synoptic disturbances. On the other hand, in the beaching case (Fig. 5b), the particles are trapped along the east coast of Sakhalin from 49 to 54°N. Consequently, the number of particles that spread offshore of Sakhalin is reduced. These two results suggest that the particles deployed in April cannot be transported south of the Sakhalin Island regardless of the beaching effect, because of the weak ESC.

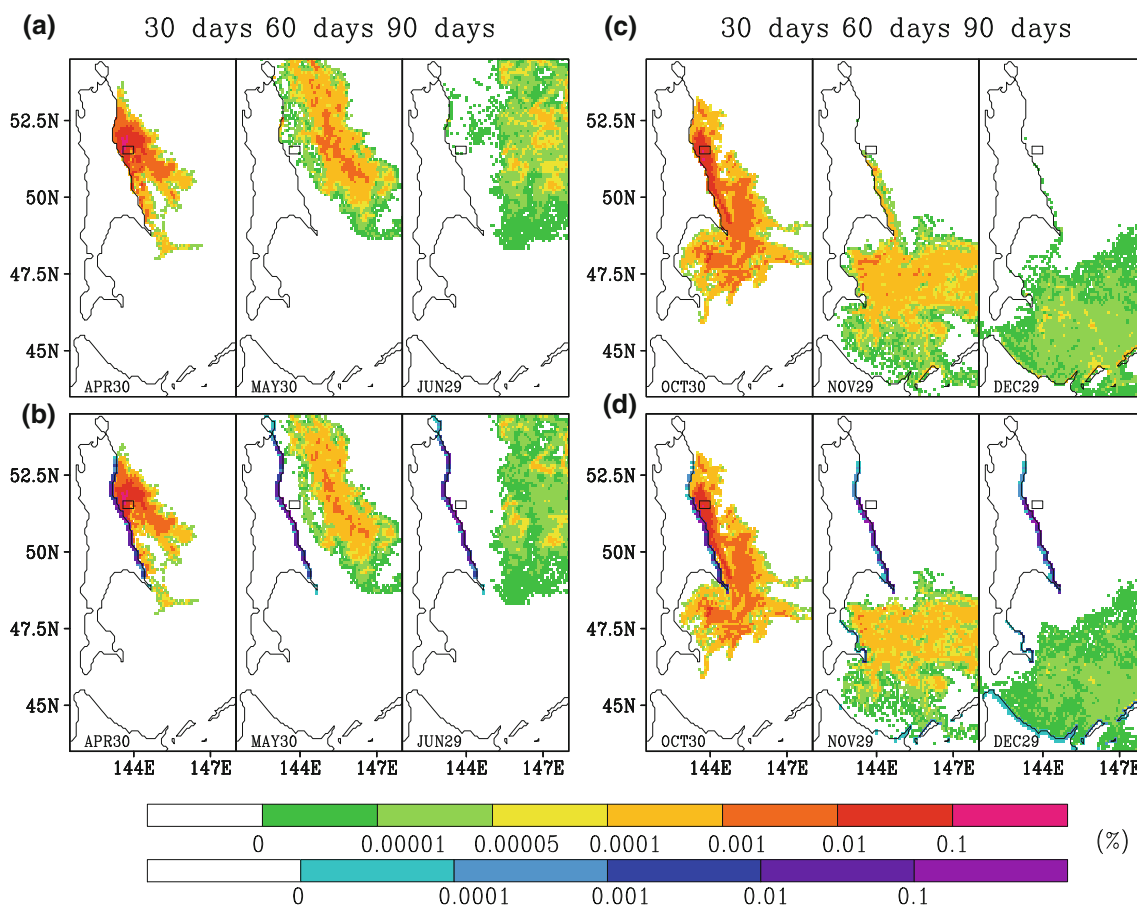


Fig. 5 Simulated time series of relative concentration at the surface after 30, 60, and 90 days in the case of April (a, b) and October (c, d) deployments, averaged for the 8 years, obtained by the particle-tracking experiment in which the total of 15,000 particles were released from the Sakhalin II (designated by a *rectangular*, also

shown by box A in Fig. 1). *Upper (a, c) and lower (b, d) panels* show the results without and with the beaching effect, respectively. *Upper color bar scale* shows the relative concentration in the water and *lower one* shows the relative concentration of beached particle (color figure online)

Figure 5c, d shows the case of October deployment. In the non-beaching case (Fig. 5c), in accordance with the abrupt intensification of the ESC in October, the particles pass through the Terpeniya Cape (see Fig. 1 for the location) and arrive south of Sakhalin Island after 30 days, while a part of the particles spread off shoreward for the westerly-dominated years. Finally, the particles are transported offshore of Hokkaido after 60–90 days. This agrees with the results of particle-tracking experiments by Ohshima and Simizu (2008). In the beaching case (Fig. 5d), the particles are trapped along the east coasts of northern and southern Sakhalin. Although the number of particles that arrive offshore of Hokkaido is reduced to some extent, the beached particles are also seen along the coasts of Hokkaido and Kuril Islands, because of the strong southward ESC.

To examine the dependence of the drift/diffusion on deployment month, we conducted particle-tracking experiments without and with the beaching effect for every

month of deployment. The relative concentrations after 90 days in January, April, July, and October–December without and with the beaching effect are shown in Fig. 6a, b, respectively. In the non-beaching case (Fig. 6a), a part of particles arrives offshore of Hokkaido in the strong ESC period (October–January). By contrast, the particles released in April and July are mostly diffused offshoreward by the synoptic wind drift before the intensification of the ESC, and do not extend to the southern part of the Sea of Okhotsk. In the beaching case (Fig. 6b), regardless of the deployment month, many particles beach along the Sakhalin coast north of the Terpeniya Cape. In the December and January cases, large numbers of particles tend to beach on the Sakhalin coast because of relatively strong synoptic disturbance seasons, and thus the particle distributions are quite different from those in the non-beaching case. These features were also seen in February and March (not shown). The largest difference is shown in the January deployment case, where most of the particles are trapped

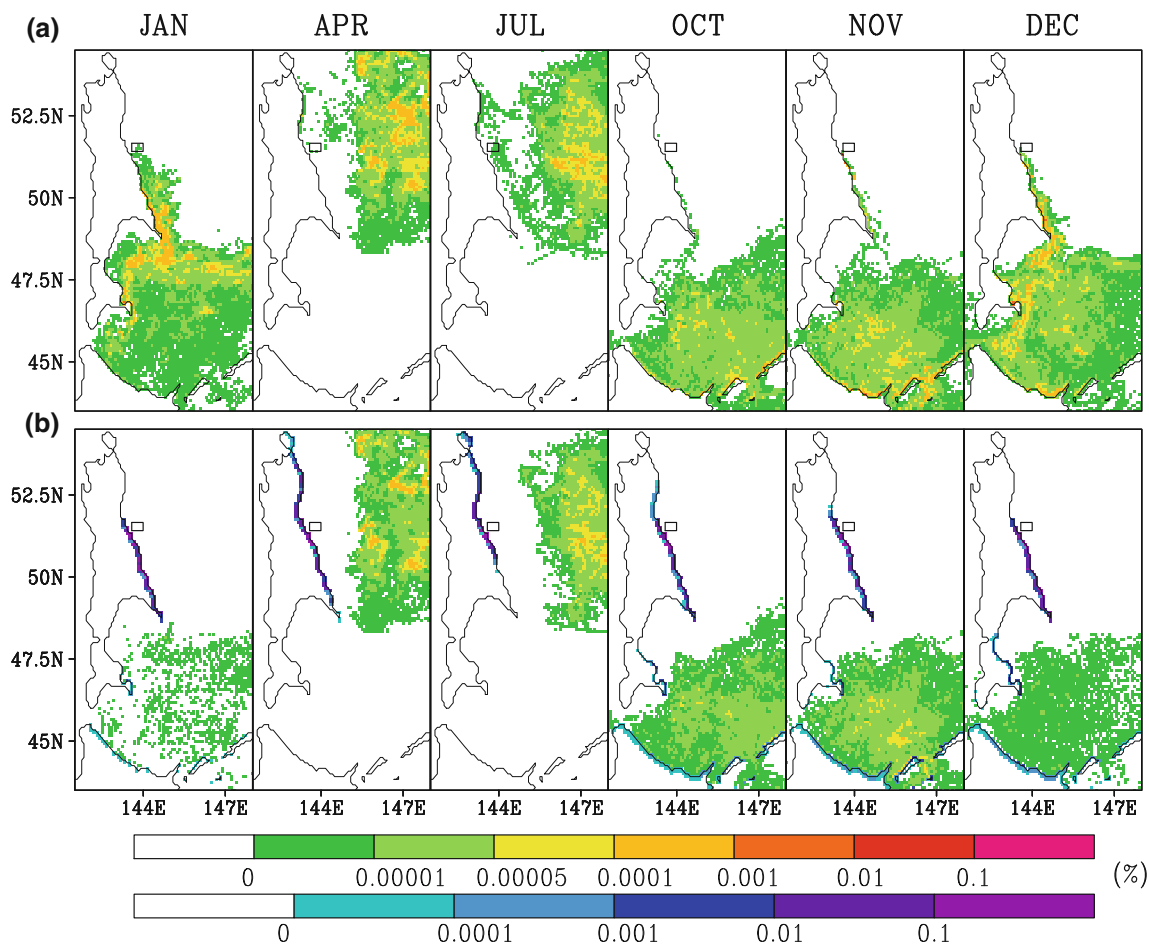


Fig. 6 Simulated relative concentration at the surface after 90 days for January, April, July, October, November, and December deployments, averaged for the 8 years, obtained by the particle-tracking experiment in which the total of 15,000 particles were released from

the Sakhalin II (designated by a *rectangle*, also shown by box A off Sakhalin in Fig. 1). *Upper (a)* and *lower (b)* panels show the results without and with the beaching effect, respectively

along the Sakhalin coast in the beaching case. In reality, the beaching effect depends on the character of the coastal zone and the properties of the spilled oil, and the realistic relative concentration distribution is considered to lie between Fig. 6a and b. Even though the particles reach the Hokkaido coast, since the half-life of evaporation (~ 1 days) and biodegradation (~ 10 days) is shorter than the transporting time of particle arrivals offshore of Hokkaido (60–90 days), the relative concentration there would decrease to $\sim 10^{-4}$ %. In any cases of September–January deployment, followed by the strong ESC period, the particles would arrive the Hokkaido coast after 60–90 days.

Here, we defined the amount of spilled oil per 1 km^2 as P , represented by $MD/100A$, where M (kl) is the total amount of spilled oil, D (%) is the relative (tracer) concentration at a certain grid cell, and A (km^2) is the area of the grid cell, $\sim 50 \text{ km}^2$. It is difficult to predict the amount of spilled oil from an accident at the Sakhalin II. Here, we assumed $M = 50,000$ kl, which is the same value for the case of Prigorodnoye (Sect. 4.3). This value is based on the worst case of the tanker accident that would happen off Prigorodnoye. Using this value, P is estimated to be $100\text{--}1,000 \text{ l km}^{-2}$ around the Sakhalin II after 30 days, while P is reduced to 1 l km^{-2} offshore of Hokkaido after 90 days, in the cases of October–January deployment. Next, we defined the amount of beached oil per unit of coast Q , represented by $MD/100L$, where L (km) is the length of coast that is assumed to be parallel to one side of a grid cell, ~ 10 km. In the October–January deployment cases, the estimated Q is $50\text{--}5,000 \text{ l km}^{-1}$ along the east Sakhalin coast and 5 l km^{-1} along the Hokkaido coast.

4.3 Particle-tracking simulations off Prigorodnoye

Prigorodnoye (cross in Fig. 1) located in the eastern coast of Aniva Bay is the tanker terminal at the end of oil and gas pipelines from the Sakhalin II. The probability of an oil spill incident is relatively high, because of heavy traffic of the oil tanker. Hence, we carried out particle-tracking simulations with the particles released in the region off Prigorodnoye.

Figure 7a, b shows the simulated relative concentrations at the surface after 10, 20, and 40 days in the case of April deployment, where the total of 15,000 particles were released from the region (box B in Fig. 1). In the non-beaching case (Fig. 7a), the particles drift and diffuse over the whole area of Aniva Bay after 10 days. This is caused mainly by the drift effect due to synoptic wind. Even after 20 days, most particles tend to remain in Aniva Bay because of the weak current speed conditions in this season (Fig. 4). After 40 days, a part of them are carried offshore of Hokkaido by the SWC, while a part of them are transported eastward by the anticyclonic gyre in the Kuril Basin.

In the beaching case (Fig. 7b), the particles are trapped along the western coast of Aniva Bay and the coast of Hokkaido. A part of them are also transported by the anticyclonic gyre in the Kuril Basin after 40 days (Fig. 7b).

Figure 7c, d shows the case of October deployment. In the non-beaching case (Fig. 7c), the particles spread from Aniva Bay after 10 days by relatively strong wind drift and then some of them are transported towards the Shiretoko Peninsula (see Fig. 1 for the location) via the strong southeastward SWC, with a covering over the offshore of Hokkaido after 20–40 days. In the beaching case (Fig. 7d), the particles beach on the Hokkaido coast after 40 days, in addition to the coasts of Aniva Bay.

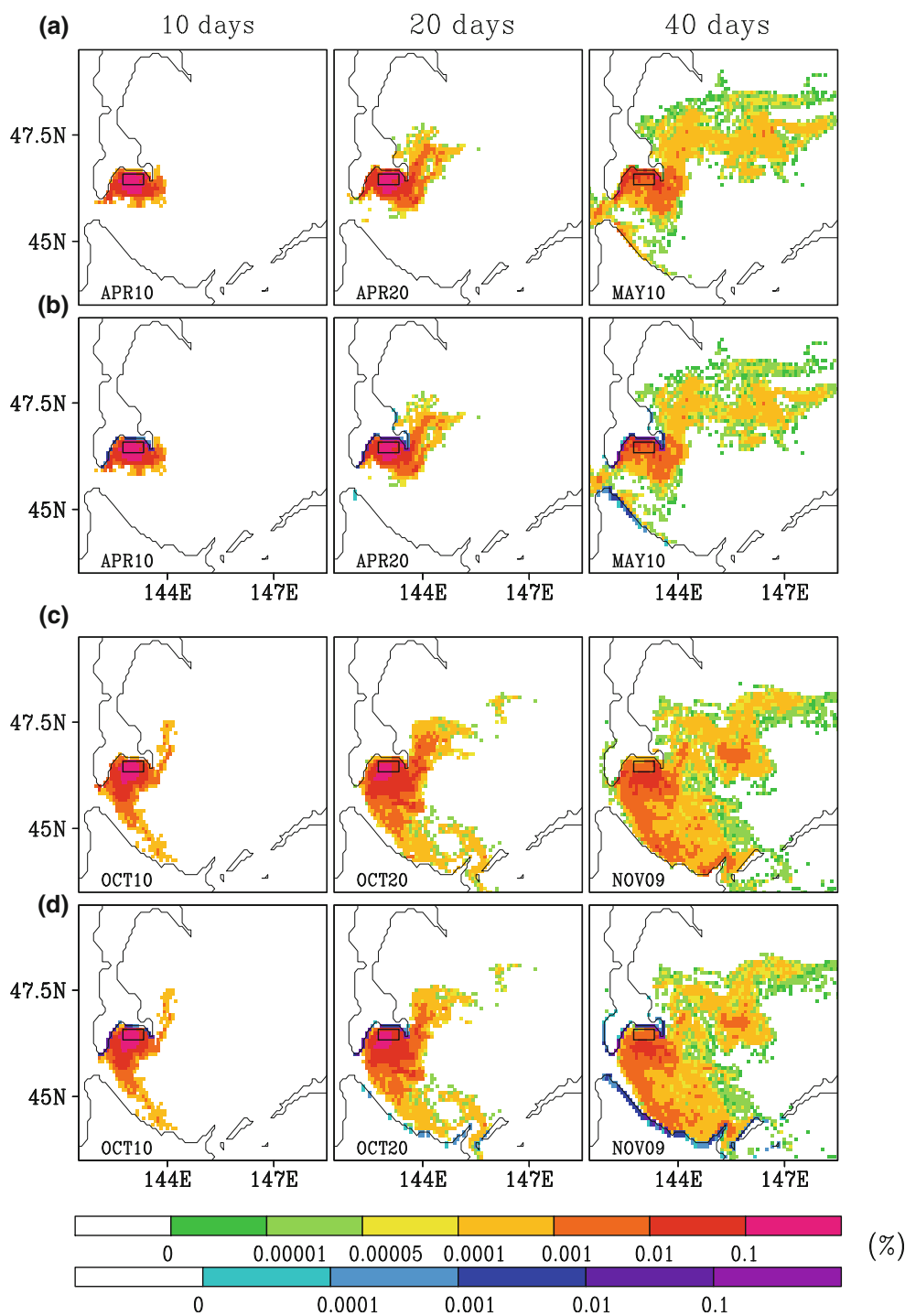
To investigate the dependence of the drift/diffusion on deployment month, we carried out particle-tracking experiments without and with the beaching effect for every month of deployment. The relative concentrations after 40 days in January, April, July, and October–December without and with the beaching effect are shown in Fig. 8a and b, respectively. For most of the non-beaching cases, except for the periods from November to February when the ESC is strong, some of the particles from Aniva Bay are transported northward and then eastward by the anticyclonic gyre in the Kuril Basin (April, July, and October in Fig. 8a). Although this feature can also be seen in the beaching case (Fig. 8b), the number of the particles transported are reduced since most particles beach the coast of Aniva Bay. In the beaching case (Fig. 8b), regardless of the deployment month, relatively large number of the particle beaches in Aniva Bay. In the cases of October–January deployment, after the diffusion by the synoptic wind drift, a part of the particles are also transported to the Shiretoko Peninsula along the Hokkaido coast by the SWC in October–December and by the ESC in January. In the November–April deployment cases, some of the particles flow out to the Japan Sea through the Soya Strait regardless of the beaching effect (Fig. 8a, b). The outflow to the Japan Sea will be discussed in the next section.

Here, we estimated the amounts of spilled oil per 1 km^2 as P , or the beached oil per unit of coast Q , as in Sect. 4.2. When the amount of oil released from a tanker off the Prigorodnoye is 50,000 kl in the October–January deployment cases, an amount of $1\text{--}100 \text{ l km}^{-2}$ reaches the region offshore of Hokkaido, while $50\text{--}5,000 \text{ l km}^{-1}$ beaches along the Hokkaido coast, after 40 days. These amounts are larger than those from the Sakhalin II by one to three orders of magnitude.

4.4 Effects of tidal currents

In Sects. 4.2 and 4.3, we performed a series of particle-tracking experiments explicitly including diurnal tidal currents (K_1 and O_1). Here, we examined the tidal effects

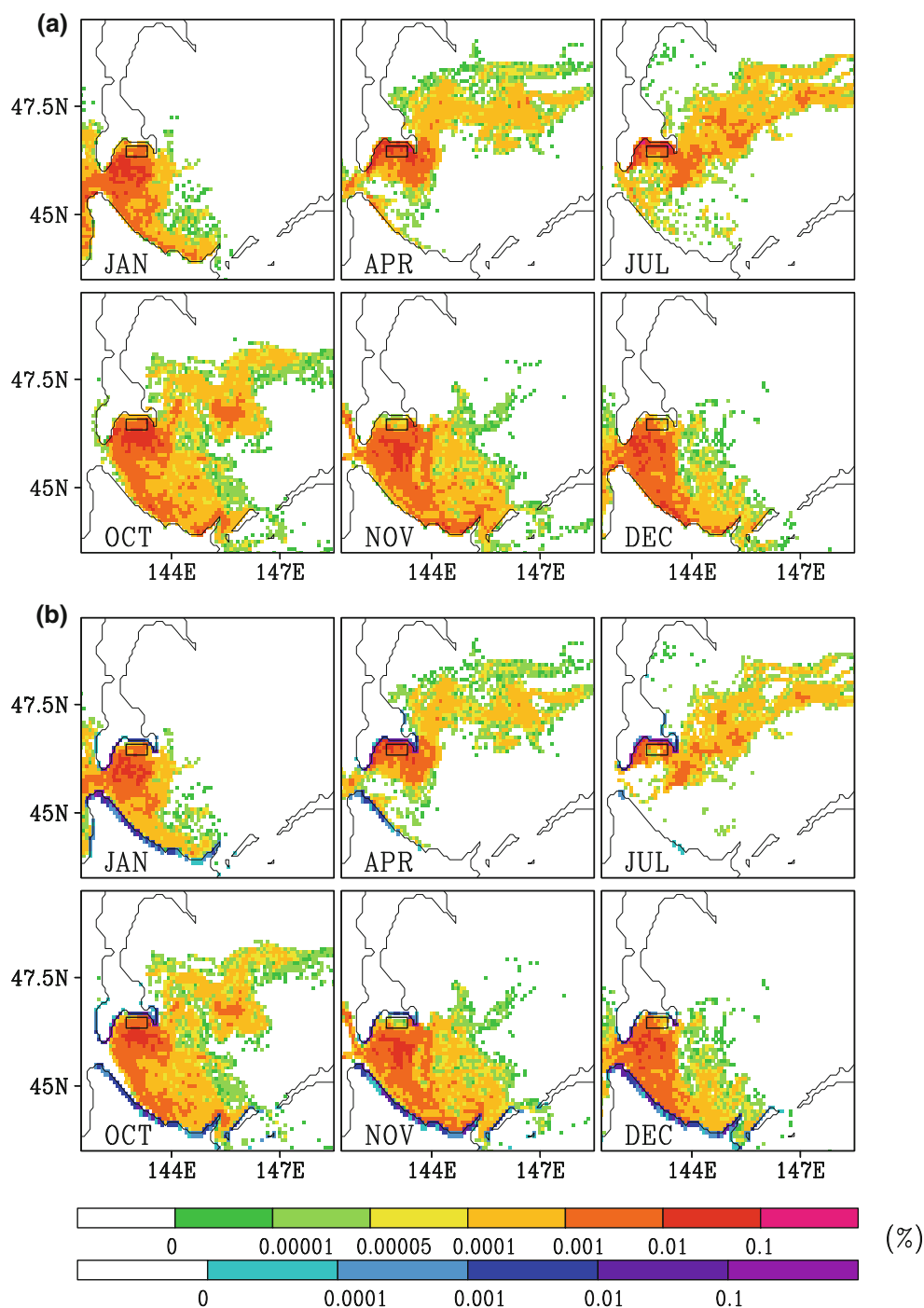
Fig. 7 Simulated time series of relative concentration at the surface after 10, 20, and 40 days in the case of April (a, b) and October (c, d) deployments, averaged for the 8 years, obtained by the particle-tracking experiment in which the total of 15,000 particles were released from the region off Prigorodnoye (designated by a rectangle, also shown by box B in Fig. 1). In (a, c) and (b, d), the results without and with beaching effect are shown, respectively



on the behavior of the particles. Figure 9a, b shows the simulated relative concentrations with and without tidal currents (K_1 and O_1) after 90 days in the case of January deployment from the Sakhalin II without the beaching effect. In the absence of tidal currents, the relative concentration of particles that are carried offshore of Hokkaido by the ESC is found to be reduced in comparison with that with the tidal currents (Fig. 9a, b). When the tidal currents are included, the southward transportation is somewhat

enhanced (Fig. 9c), and the increased speed is roughly estimated to be 100 km per 90 days ($\sim 1 \text{ km day}^{-1}$) from the difference in the high concentration area between Fig. 9a and b. The tidal-induced Stokes drift is calculated to be southward over the Sakhalin shelf with the relatively larger drift being $\sim 1 \text{ km day}^{-1}$ ($\sim 1 \text{ cm s}^{-1}$) at the northern shelf and Terpeniya Bay, where the tidal currents are strong (Fig. 9d). From the theory of Longuet-Higgins (1969), assuming that the current changes in the cross-

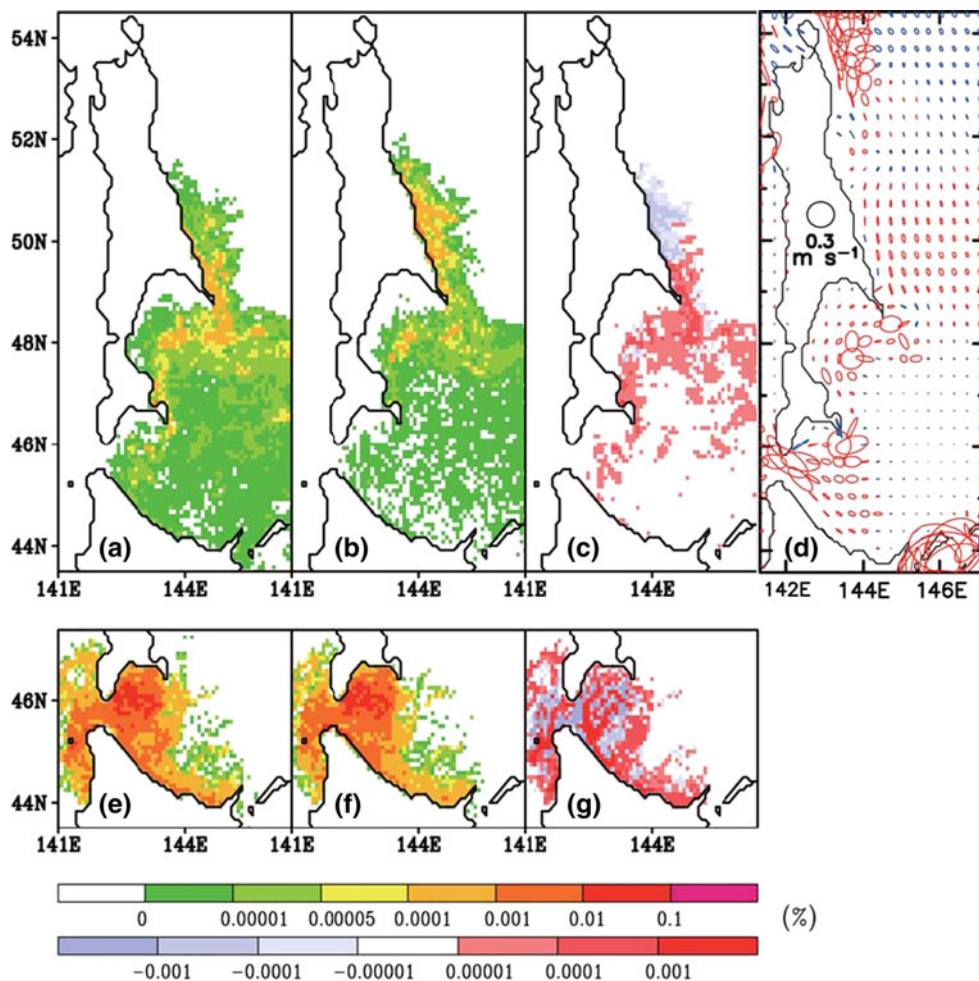
Fig. 8 Simulated relative concentration at the surface after 40 days for January, April, July, October, November, and December deployments, averaged for the 8 years, obtained by the particle-tracking experiment in which the total of 15,000 particles were released from the region off Prigorodnoye, **a** without and **b** with the beaching effect



isobath direction are small, the typical magnitude of the Stokes drift is represented by $V_T^2/2C_T$, where V_T is the scale of tidal velocity and C_T is the phase speed of the tidal wave. When typical values of $V_T \sim 0.3 \text{ m s}^{-1}$ and $C_T \sim 5 \text{ m s}^{-1}$ are used, the Stokes drift is estimated to be $\sim 1 \text{ cm s}^{-1}$, which is comparable to the model result. Thus, the enhancement of the southward transport is attributed in part to the tidal-induced Stokes drift. Similar southward

enhancement by the tidal currents are also seen in the October–December deployment cases, when the ESC is strong. It is also noted that the Eulerian residual currents are southward with 1–2 cm s^{-1} in the eastern coast of Sakhalin (Kowalik and Polyakov 1998). Although this effect is not included in the present study, it would also contribute to the enhancement of the southward transport. In March–August when the ESC is weak, the deployed

Fig. 9 *Top panels* show the simulated relative concentration **a** with and **b** without the tidal currents, after 90 days in the case of January deployment from the Sakhalin II. **c** The difference of (a–b). **d** The most dominant K_1 tidal current ellipses from the three-dimensional tidal model (Ono and Ohshima 2010), where the rotation direction for clockwise and counterclockwise is indicated by *red* and *blue*, respectively. *Bottom panels* show the simulated relative concentration **e** with and **f** without the tidal currents, after 40 days in the case of January deployment from the region off Prigorodnoye. **g** The difference of (e–f). In (c and g), *warm* and *cold colors* denote the increase and decrease, respectively, in the relative tracer concentration due to the tidal effects (color figure online)



particles are hardly affected by tidal currents because the particles are diffused offshoreward by the wind drift due to synoptic disturbances.

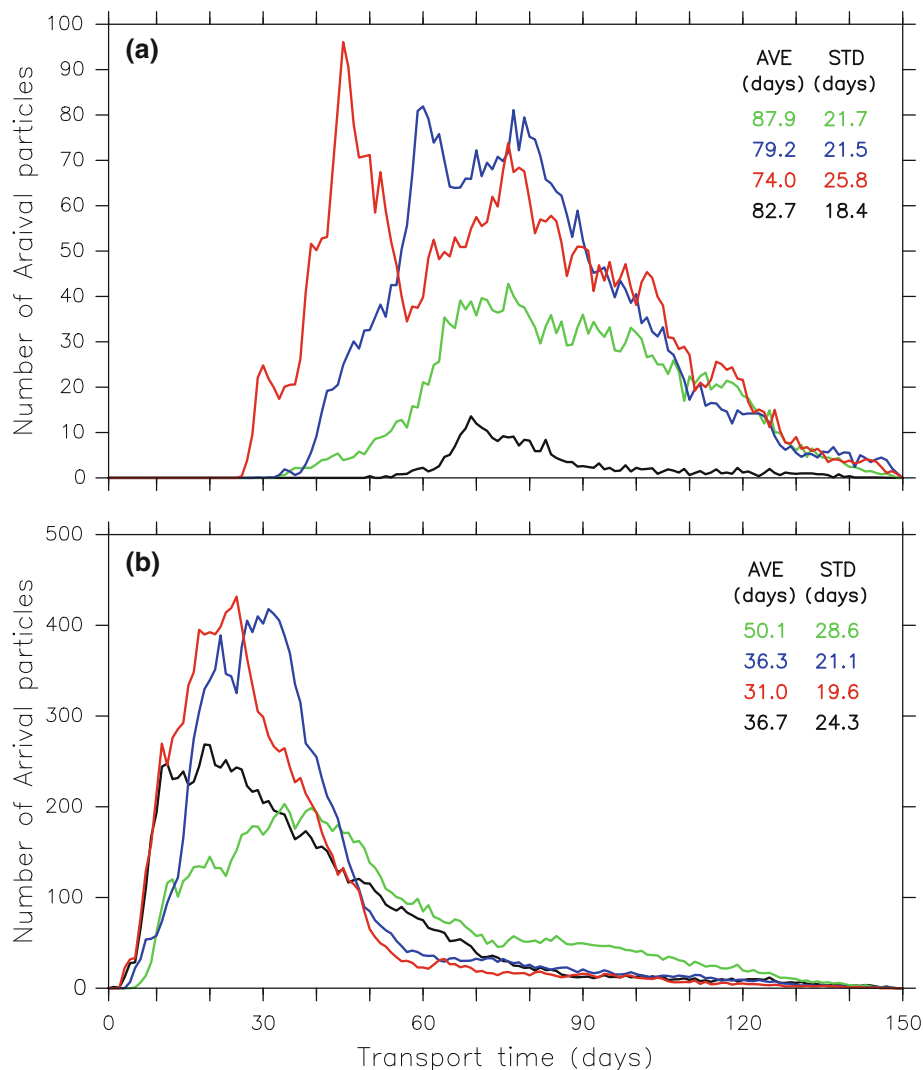
Figure 9e, f shows the simulated relative concentration with and without tidal currents, after 40 days in the case of January deployment from the region off Prigorodnoye. A part of the particles flow out to the Japan Sea regardless of the presence of the tidal currents, but the rate of flowing out to the Japan Sea is increased by the tidal currents (Fig. 9g). In January, the wind drift by the synoptic wind is very strong and this mainly causes the outflow to the Japan Sea (Fig. 3). The effect of the tidal currents is secondary to the outflow. In simulating the drift/diffusion of spilled oil, the inclusion of tidal current likely provides a more reliable simulation, as shown, although its effect is not dominant.

4.5 Transporting time to the Hokkaido coast

In the behavior of the spilled oil, the evaporation and biodegradation depend on the weather conditions and oil properties, and thus their parameters used in the present

study include uncertainty. For the environmental risk assessment of the spilled oil on the Hokkaido coast, estimation of the transporting time of the particles from the source regions is the basic information, regardless of parameters for evaporation and biodegradation. In this section, assuming the worst-case scenario, we estimated the transporting time of the particles to the Hokkaido coast from the Sakhalin II and the region off Prigorodnoye, and examined its dependence on the deployment month, based on the particle-tracking experiments without the beaching. It is noted that the effects of evaporation and biodegradation are not included in this analysis in order to focus only on the transporting time. We defined the transporting time for a certain particle as the time that the particle first enters a grid cell adjacent to the Hokkaido coast from 141.5 to 145.5°E. On the basis of the results from 1998 to 2005, we constructed the histogram of the transporting time of the particles, averaged over 8 years. In Fig. 10, we show the results for October–January deployments, when relatively large number of particles reach the Hokkaido coast. In the case from the Sakhalin II (Fig. 10a), the December

Fig. 10 Histogram of the transport time of particles from **a** Sakhalin II and **b** Prigorodnoye to the Hokkaido coast, for October (*green*), November (*blue*), December (*red*), and January (*black*) deployments, obtained by the particle-tracking experiment without the beaching effect. Values averaged over 8 years are plotted. The average (*AVE*) and standard deviation (*STD*) of the transporting time in each month are also indicated (color figure online)



deployment has the fastest transporting time of 25 days, while in the case from the region off Prigorodnoye (Fig. 10b), the transporting time is much shorter, only 3 days in the November–January deployment cases.

5 Concluding remarks

On the basis of the model by Uchimoto et al. (2007), we developed a three-dimensional, high-resolution ocean circulation model for the Sea of Okhotsk by comparing all the available new and historical data. We believe that the present model is the best model that reproduces the realistic current fields in the Sea of Okhotsk to date. This model improved the velocity field during the strong stratification period, for which the performance of the previous model such as Ohshima and Simizu (2008) is relatively poor. Since the model includes the water exchange with the Japan Sea, it reasonably represents the SWC entering into the Sea of Okhotsk from the Japan Sea. For the drift/diffusion

simulation off the Sakhalin and Hokkaido coasts, our model is considered to provide reliable results. This study carried out particle-tracking experiments in which the particles are deployed from the Sakhalin II and the region off Prigorodnoye, toward the oil spill simulation in the Sea of Okhotsk. The results are shown by the relative concentration averaged over the 8 years of 1998–2005 based on the ensemble forecast idea.

In the case from the Sakhalin II, the particles deployed in September–January are transported southward by the ESC, finally arriving at the coast of Hokkaido after 60–90 days. By contrast, the particles deployed in March–August are diffused offshore by the synoptic wind drift rather than being trapped by the mainstream of the ESC, and thus the particles are hardly transported to regions south of Sakhalin. In the presence of the beaching effect, the particles released in March–August are beached on the Sakhalin coast north of Terpeniya Bay. The particles released in October–December when the ESC is strong can reach the coasts of Sakhalin, Hokkaido, Kunashiri, and Etorofu

(see Fig. 1 for the locations), regardless of the beaching effect. Since the half-life of evaporation (~ 1 days) and biodegradation (~ 10 days) is shorter than the transporting time of particle to the offshore of Hokkaido (60–90 days), the relative concentration there would be considerably smaller. If the oil of 50,000 kl is released from the Sakhalin II, after 90 days, the spilled and beached oil are reduced to 1 l km^{-2} and 5 l km^{-1} around Hokkaido, respectively.

In the case from the region off Prigorodnoye, the particles spread in the whole area of Aniva Bay regardless of the deployment month. Then, a part of them are transported eastward by the anticyclonic circulation in the Kuril Basin, while a part of them are carried offshore of Hokkaido by the SWC. In the cases of September–January deployment, a part of particles after 40 days can be transported to the Shiretoko Peninsula with a large part of particles flowing along the Hokkaido coast by the SWC in October–December and by the ESC in January. If the same amount of oil is released from the Sakhalin II and Prigorodnoye, the amounts of spilled and beached oil around Hokkaido are larger in the case of Prigorodnoye than those in the case of Sakhalin II by one to three orders of magnitude. This is mainly because the transporting time of particles to the offshore of Hokkaido is shorter in the case of Prigorodnoye (~ 40 days) than in the case of Sakhalin II (~ 90 days). The particles deployed in November–April tend to flow out to the Japan Sea through the Soya Strait. The outflow to the Japan Sea is mainly caused by the synoptic wind drift under the weakening of the SWC. The diffusion by the strong tidal currents around the Soya Strait is the second contributor to the outflow.

In our particle-tracking experiments, we parameterized the effects of evaporation and biodegradation on the spilled oil by a simple method that shows that the relative concentration is exponentially decreased with time. However, the evaporation and biodegradation processes depend on oil components, temperature, wind speed, and biomass. Therefore, high-accuracy parameterization (e.g., Wang et al. 2008; Guo and Wang 2009) is needed for more realistic oil spill simulation. In the Sea of Okhotsk, Yamaguchi et al. (2010) have carried out more realistic simulation for spilled oil in the ice-covered seasons focusing on the offshore of Hokkaido, based on the velocities of our dataset. According to their numerical model, forecasts of the spilled oil distribution up to 1 week ahead are possible by giving the time, place, and amount of the spilled oil as the input data. Their model also showed that the drift/diffusion of the spilled oil are determined by the ocean current to the zeroth order approximation.

Acknowledgments We would like to thank Masaaki Wakatsuchi for his encouragement and Daisuke Simizu for his advice and support. We also thank Akira Kurokawa of the Engineering Advancement

Association of Japan (ENAA) and Naoki Nakazawa of the Systems Engineering Associates, Inc. for their supports. Comments by the editor and anonymous two reviewers helped improve the paper. This study was supported by ENAA. All the simulations were calculated by HITACHI SR-11000 supercomputer at the Hokkaido University Computing Center.

References

- Aota M (1975) Studies on the Soya Warm Current. *Low Temper Sci Ser A* 33:151–172 (in Japanese with English abstract)
- Csanady GT (1978) The arrested topographic wave. *J Phys Oceanogr* 8(1):47–62
- Ebuchi N, Fukamachi Y, Ohshima KI, Shirasawa K, Ishikawa M, Takatsuka T, Daibo T, Wakatsuchi M (2006) Observation of the Soya Warm Current using HF ocean radar. *J Oceanogr* 62(1):47–61. doi:10.1007/s10872-006-0031-0
- Ebuchi N, Fukamachi Y, Ohshima KI, Wakatsuchi M (2009) Subinertial and seasonal variations in the Soya Warm Current revealed by HF ocean radars, coastal tide gauges, and bottom-mounted ADCP. *J Oceanogr* 65(1):31–43. doi:10.1007/s10872-009-0003-2
- Fukamachi Y, Tanaka I, Ohshima KI, Ebuchi N, Mizuta G, Yoshida H, Takayanagi S, Wakatsuchi M (2008) Volume transport of the Soya Warm Current revealed by bottom-mounted ADCP and ocean-radar measurement. *J Oceanogr* 64(3):385–392. doi:10.1007/s10872-008-0031-3
- Fukamachi Y, Ohshima KI, Ebuchi N, Bando T, Ono K, Sano M (2010) Volume transport in the Soya Strait during 2006–2008. *J Oceanogr* 66(5):685–696. doi:10.1007/s10872-010-0056-2
- Guo WJ, Wang YX (2009) A numerical oil spill model based on a hybrid method. *Mar Pollut Bull* 58:726–734
- Kakinuma T, Yanagi T (1976) Oil spreading from Mizushima Harbor. In: Proceedings of 23rd conference on coastal engineering, JSCE, pp 559–563 (in Japanese)
- Kerr RA, Kintisch E, Schenkman L, Stokstad E (2010) Five questions on the spill. *Science* 328(5981):962–963. doi:10.1126/science.328.5981.962
- Korotenko KA, Mamedov RM, Kontar AE, Korotenko LA (2004) Particle tracking method in the approach for prediction of oil slick transport in the sea: modelling oil pollution resulting from river input. *J Mar Syst* 48:159–170
- Kowalik Z, Polyakov I (1998) Tides in the Sea of Okhotsk. *J Phys Oceanogr* 28(7):1389–1409
- Large WG, Pond S (1981) Open ocean momentum flux measurements in moderate to strong winds. *J Phys Oceanogr* 11(3):324–336
- Levitus S, Burgett R, Boyer TP (1994) Salinity. *World Ocean Atlas 1994*. NOAA Atlas NESDIS, 3
- Longuet-Higgins MS (1969) On the transport of mass by time-varying ocean currents. *Deep Sea Res I* 16:431–447
- Mellor GL, Yamada T (1982) Development of a turbulence closure model for geophysical fluid problems. *Rev Geophys Space Phys* 20:851–875
- Mellor GL, Ezer T, Oey L-Y (1994) The pressure gradient conundrum of sigma coordinate ocean models. *J Atmos Ocean Technol* 11:1126–1134
- Mellor GL, H“akkinen S, Ezer T, Patchen R (2002) A generalization of a sigma coordinate ocean model and an intercomparison of model vertical grids. In: Pinnardi N, Woods JD (eds) *Ocean forecasting conceptual basis and applications*, Springer, Berlin, pp 55–72
- Miyazawa Y, Guo X, Yamagata T (2004) Roles of mesoscale eddies in the Kuroshio paths. *J Phys Oceanogr* 34(10):2203–2222

- Mizuta G, Fukamachi Y, Ohshima KI, Wakatsuchi M (2003) Structure and seasonal variability of the East Sakhalin Current. *J Phys Oceanogr* 33(11):2430–2445
- Ogi M, Tachibana Y, Nishio F, Danchenkov MA (2001) Does the fresh water supply from the Amur River flowing into the Sea of Okhotsk affect sea ice formation? *J Meteorol Soc Jpn* 79(1):123–129. doi:10.2151/jmsj.79.123
- Ohshima KI (1994) The flow system in the Japan Sea caused by a sea level difference through shallow straits. *J Geophys Res* 99(C5):9925–9940. doi:10.1029/94JC00170
- Ohshima KI, Wakatsuchi M (1990) A numerical study of barotropic instability associated with the Soya Warm Current in the Sea of Okhotsk. *J Phys Oceanogr* 20(4):570–584
- Ohshima KI, Simizu D (2008) Particle tracking experiments on a model of the Okhotsk Sea: toward oil spill simulation. *J Oceanogr* 64(1):103–114. doi:10.1007/s10872-008-0008-2
- Ohshima KI, Wakatsuchi M, Fukamachi Y, Mizuta G (2002) Near-surface circulation and tidal currents of the Okhotsk Sea observed with satellite-tracked drifters. *J Geophys Res* 107(C11):3195. doi:10.1029/2001JC001005
- Ohshima KI, Simizu D, Itoh M, Mizuta G, Fukamachi Y, Riser SC, Wakatsuchi M (2004) Sverdrup balance and the cyclonic gyre in the Sea of Okhotsk. *J Phys Oceanogr* 34(2):513–525
- Ohshima KI, Ono J, Simizu D (2008) Particle tracking experiments for drifting materials on a model of the Sea of Okhotsk. *Bull Coast Oceanogr* 45(2):115–124 (in Japanese with English abstract)
- Ohshima KI, Nakanowatari T, Riser S, Wakatsuchi M (2010) Seasonal variation in the in- and outflow of the Okhotsk Sea with the North Pacific. *Deep Sea Res II* 57(13–14):1247–1256. doi:10.1016/j.dsr2.2009.12.012
- Ono J, Ohshima KI (2010) Numerical model studies on the generation and dissipation of the diurnal coastal-trapped waves over the Sakhalin shelf in the Sea of Okhotsk. *Cont Shelf Res* 30(6):588–597. doi:10.1016/j.csr.2009.06.006
- Ono J, Ohshima KI, Mizuta G, Fukamachi Y, Wakatsuchi M (2008) Diurnal coastal-trapped waves on the eastern shelf of Sakhalin in the Sea of Okhotsk and their modification by sea ice. *Cont Shelf Res* 28(6):697–709. doi:10.1016/j.csr.2007.11.008
- Petroleum Association of Japan (2005) Diffusion/drift prediction model for spilled oil: the Okhotsk Sea Version. V. 7.1, Users Manual (in Japanese)
- Shen HT, Yapa PD (1988) Oil slick transport in rivers. *J Hydraul Eng* 114(5):529–543
- Simizu D, Ohshima KI (2006) A model simulation on the circulation in the Sea of Okhotsk and the East Sakhalin Current. *J Geophys Res* 111:C05016. doi:10.1029/2005JC002980
- Smagorinsky J (1963) General circulation experiments with the primitive equations: Part I. The basic experiment. *Mon Weather Rev* 91(3):99–164
- Uchimoto K, Mitsudera H, Ebuchi N, Miyazawa Y (2007) Anticyclonic eddy caused by the Soya Warm Current in an Okhotsk OGCM. *J Oceanogr* 63(3):379–391. doi:10.1007/s10872-007-0036-3
- Varlamov SM, Yoon J-H (2003) Operational simulation of oil spill in the Sea of Japan. *Rep Res Inst Appl Mech Kyushu Univ* S1:15–20
- Varlamov SM, Yoon J-H, Hirose N, Kawamura H, Shiohara K (1999) Simulation of the oil spill processes in the Sea of Japan with regional ocean circulation model. *J Mar Sci Technol* 4:94–107
- Wang S-D, Shen Y-M, Guo Y-K, Tang J (2008) Three-dimensional numerical simulation for transport of oil spills in seas. *Ocean Eng* 35(5–6):503–510.
- Watanabe T, Ikeda M, Wakatsuchi M (2004) Thermohaline effects of the seasonal sea ice cover in the Sea of Okhotsk. *J Geophys Res* 109:C09S02. doi:10.1029/2003JC001905
- Yamaguchi H, Ono J, Ohshima KI, Kurokawa A (2010) A system for numerical prediction of spilled oil behavior in the Sea of Okhotsk including ice-covered condition. In: Proceedings of 25th international symposium on Okhotsk Sea and Sea Ice, pp 17–24 (in Japanese with English abstract)
- Yanagi T, Okamoto Y (1984) A numerical simulation of oil spreading on the sea surface. *La Mer* 22:137–146